Buckled Two-Dimensional Xene Sheets

Alessandro Molle[1], Joshua Goldberger[2], Michel Houssa[3], Yong Xu[4,5,6], Shou-Cheng Zhang[7,8,9], and Deji Akinwande[10]

[1] Laboratorio MDM, IMM-CNR, via C. Olivetti 2, Agrate Brianza, I-20864, Italy
[2] Department of Chemistry and Biochemistry, The Ohio State University, Columbus, OH 43210, USA
[3] Department of Physics and Astronomy, University of Leuven, B-3001 Leuven, Belgium
[4] State Key Laboratory of Low Dimensional Quantum Physics, Department of Physics, Tsinghua University, Beijing 100084, People's Republic of China
[5] Collaborative Innovation Center of Quantum Matter, Beijing 100084, People's Republic of China
[6] RIKEN Center for Emergent Matter Science (CEMS), Wako, Saitama 351-0198, Japan
[7] Department of Physics, McCullough Building, Stanford University, Stanford, California 94305-4045, USA
[8] Stanford Institute for Materials and Energy Sciences, SLAC National Accelerator Laboratory, Menlo Park, California 94025, USA
[9] Institute for Advanced Study, Tsinghua University, Beijing 100084, People's Republic of China
[10] Microelectronics Research Center, The University of Texas at Austin, Texas 78758, USA

Abstract

Silicene, germanene, and stanene, are part of a monoelemental class of two-dimensional (2D) crystals termed 2D-Xenes (X=Si, Ge, Sn) which, together with their ligand-functionalized derivatives referred to as Xanes, are comprised of group IVA atoms arranged in a honeycomb lattice – similar to graphene but with varying degrees of buckling. Their electronic structure range from trivial insulators, to semiconductors with tunable gaps, to semimetallic, depending on the substrate, chemical functionalization, and strain. More than a dozen different topological insulator states are predicted to emerge, including the quantum spin Hall state at room temperature, which, if realized, would enable new classes of nanoelectronic and spintronic devices, such as the topological field effect transistor. The electronic structure can be tuned, for example, by changing the group IVA element, the degree of spin-orbit coupling, the functionalization chemistry, or the substrate, making the 2D-Xene systems promising multifunctional 2D materials for nanotechnology. This Perspective Article highlights the current state-of-the art and future opportunities in the manipulation and stability of these materials, their functions and applications, and novel device concepts.

55 The rise of graphene has inspired the flourish of a so-called "flatland" of two-
56 dimensional (2D) materials with complementary properties and functionalities enabling
57 rapid advances in science and engineering, and an accelerated global development in
58 nanotechnology applications that can address societal challenges in energy, electronics,
59 sensors and health.[1,2,3] One closely related class of 2D crystals are the single-element
60 "2D-Xenes", which take their etymology from the sp^2-hybridized alkene bond and are
61 generally comprised of a single-layer of atoms organized into a honeycomb-like lattice.
62 In particular, 2D-Xenes made of group-IVA elements, referred to as "silicene",
63 "germanene", and "stanene" when X=Si, Ge, and Sn respectively, are isoelectronic to
64 graphene,[4] however their larger interatomic distances result in up and down atomic
65 buckling about a honeycomb lattice[5], and also afford new routes towards covalent
66 functionalization. The buckled structure and the strong spin-orbit coupling (SOC)
67 concurrently paves a pathway for accessing the new quantum state of matter known as a
68 2D topological insulator (TI), a solid-state material that has both an insulating electronic
69 structure in the bulk and dissipation-less conducting channels along the edges that are
70 protected against back-scattering by time reversal symmetry. The potential technological
71 value of such an effect is that it enables the creation of a material that exhibits ideal
72 conduction along the edges that is immune from scattering from a variety of defects and
73 disorder. Overall, intriguing questions have come to the forefront such as: What are the
74 benefits and challenges that arise owing to the intrinsic buckling and surface sensitivity in
75 2D-Xenes? And can 2D-Xenes ultimately establish topology as a paradigm shift for
76 nanoscale opto-electronics? These questions are discussed here with highlights on the
77 opportunities and perspectives on the technical challenges.

A pseudo planar flatland

While the planar flatland has been considered the norm for the past ten years as is the case for graphene and h-BN, *anisotropy* in honeycomb lattices stemming from the extended vertical distortions (for example bond buckling in 2D-Xenes or puckering in phosphorene) is now the *new normal.*[4,5,6] The native buckling can have dramatic implications in the overall physics and chemistry of the 2D-Xenes. For instance, the degree of buckling can dictate the electronic character or influence the chemical reactivity. This highlights the concept of a pseudo-planar flatland where buckling can foster a number of potential functionalities that can be readily engineered.

An in-depth view on buckling. In their most stable form, 2D-Xenes based on Si, Ge or Sn atoms adopt a buckled hexagonal honeycomb structure[6,7], unlike graphene, which is ideally flat. For example, the larger bond length in silicene (~2.28 Å) compared to graphene (~1.42 Å), prevents the Si atoms from forming strong π-bonds, thus leading to deviations away from a sp^2 hybridization.[4,8] The buckling of the Si atoms brings them closer together to enable a stronger overlap of their π-bonding p_z orbitals, resulting in a mixed sp^2-sp^3 hybridization, which stabilizes their hexagonal arrangement. The vertical buckling distance δ between the top and bottom atoms of the 2D-Xene crystal structure (**Figure 1a**) is correlated to the bond angle between the framework atoms and the hybridization of the atomic orbitals: δ increases from 0 Å in graphene to 0.85 Å in free-standing (FS) stanene, with an associated decrease of the bond angle, from 120° (pure sp^2 hybridization of C atoms) to 110° (almost pure sp^3 hybridization of Sn atoms).

2D-Xenes can be described by a four-band second-nearest neighbor tight binding Hamiltonian[9] near the K and K' points, involving a SOC term (λ_{SO}) and a staggered external electric field term (E_z),

$$H = \hbar v_F(\eta k_x \tau_x + k_y \tau_y) + \eta \tau_z \sigma_z \lambda_{SO} - \frac{\delta}{2} E_z \tau_z + \frac{\lambda_{R1}(\eta \tau_x \sigma_y - \tau_y \sigma_x)}{2} + \eta \tau_z a \lambda_{R2}(k_y \sigma_x - k_x \sigma_y), \quad (1)$$

where v_F is the Fermi velocity, η=1 for K and η=-1 for K' point, $\tau_{x,y,z}$ is the Pauli matrix for the sublattice pseudospin, σ is the Pauli matrix for the electron spin, and λ_{R1} and λ_{R2} are the first and second Rashba coupling constants, related to the nearest and second nearest neighbor hopping, respectively. E_z arises from the buckling of 2D-Xenes and allows for tunability of their electronic properties.

When the SOC is not taken into account and no electric field is applied (Kane-Mele model[10]), silicene, germanene, and stanene are predicted to be zero-gap semiconductors with linear dispersions near the K and K' Dirac points. The computed Fermi velocities in silicene and germanene are about 6×10^5 m/s,[6,11] roughly half of that for graphene. With SOC, silicene and germanene are predicted to be 2D TIs with bulk energy gaps of about 1.5-2 meV and 23.9-30 meV, respectively.[9] Stanene, owing to its stronger SOC, incorporates a 2D TI state with a sizeable energy gap of about 0.1 eV.[12,13]

The 2D-Xene experimental Odyssey. The tendency of FS 2D-Xenes to buckle is experimentally confirmed by the *epitaxial growth* of various 2D-Xene "phases" on different substrates with *commensurate* surface lattice. An extensive list of substrates serving this purpose is enumerated in **Table 1**. Experimental identification of the buckled 2D-Xene structure has been mainly based on scanning tunneling microscopy (STM)

assisted by *ab initio* atomic models. Other techniques such as angle resolved photoemission spectroscopy (ARPES) have been used to reveal the electronic structure. Starting from the ideal FS 2D-Xene lattice as predicted from *ab initio* simulations (**Figure 1a**), a historical overview of the main experimental breakthroughs is presented in **Figure 1** including the STM confirmation of silicene (**b**), closely paralleled by the chemical synthesis of germanane (**c**), and followed by the epitaxy of germanene (**d**), the realization of a silicene transistor (**e**) and the epitaxy of stanene (**f**).

The forerunner of the 2D-Xene roadmap is the epitaxial silicene on metallic substrates.[14,15-19] In particular, silicene-on-Ag(111) is interesting as a model of a buckled elemental atomic sheet due to the wealth of commensurate phases on the host Ag(111) surface.[16,17] These phases are commonly written as $n\times n/m\times m$, where $n\times n$ and $m\times m$ refer to the coincidence with the FS 2D-Xene lattice and the substrate lattice, respectively; they arise from different rotational alignment of the 2D-Xene sheet with respect to the substrate. STM topographies of the majority silicene phases are reported in **Figure 1b** along with the respective atomic structure model. This structural versatility can dramatically influence the electronic structure of each 2D-Xene phase, and is a general monolayer property of the 2D-Xene family (**Table 1**).[20] In spite of this, substrate orbitals strongly hybridize with the Si atoms, resulting in an overall metallic character of the silicene-on-metal substrate system, as follows from ARPES investigations.[11,21]

Following silicene, several STM studies have detailed the atomic arrangement of buckled germanene phases on various metallic substrates[22,23,24-26] (**Figure 1d**), and the epitaxy of stanene on Bi_2Te_3 substrates has been established soon afterwards[27] (**Figure 1f**). Most recently, the epitaxy of a 2D boron sheet, termed borophene, with a metallic character

[28,29] and of a monolayer of (silicene-like) phosphorene with semiconducting character[30] were respectively reported on Ag(111) and Au(111) substrates, thus extending the realization of 2D-Xenes to elements beyond the group IVA atoms.

Covalently functionalized 2D-Xenes. The covalent functionalization into ligand-terminated Xenes is an intriguing route towards tuning chemical, physical, and topological properties of these materials, as well as increasing their environmental stability. Here we define "Xanes" as 2D-Xene derivatives in which every atom on the framework features a covalently bound ligand, thereby removing π-bonding. These ligands directly couple to the half-filled p_z orbitals in 2D-Xenes, to produce a gapped, semiconducting band structure, and the magnitude of this band gap depends on both the framework element, and the identity of the covalent ligand.[12,31,32] Unlike Xenes, Xanes can be derived by topotactic exfoliation.[31] The first reported example of topotactic exfoliation of a single germanane sheet is shown in **Figure 1c**.

The most versatile route for preparing Xanes relies on the direct chemical conversion of structurally related layered intermetallic "Zintl" phase precursors. For example, the crystal structures of $CaSi_2$, $CaGe_2$, and $BaSn_2$, are comprised of anionic $[Si]_n^-$, $[Ge]_n^-$, and $[Sn]_n^-$ layers in a puckered honeycomb arrangement analogous to 2D-Xenes, with each layer separated by a divalent cation. These phases can be transformed directly into multi-layered van der Waals crystals of Xanes by reaction with an electrophilic species that will bond directly to the group IVA framework and a solvent that solubilizes the divalent cation. For instance, the reaction of $CaSi_2$ in aqueous HCl produces partially –H/–OH terminated silicane, a reaction first reported by Friedrich Wöhler in 1863.[33] In

aqueous acidic conditions, the Si- and Sn-based Xane frameworks become partially terminated with –OH ligands, whereas the Ge-based frameworks are completely –H terminated.[31,32] Organic-terminated Xanes can be created via a similar one-step reaction of precursor Zintl phases with alkyl halides. For instance, $GeCH_3$ has been prepared via the direct reaction of $CaGe_2$ with CH_3I.[34] Also, some Si and Ge surface functionalization routes can also graft ligands onto 2D Xanes, such as the hydrosilylation of alkenes and alkynes onto 2D silicane.[35] Other strategies for preparing Xanes include electrochemical atomic layer epitaxy, which has been shown to be a viable route towards germanane,[36] as well as the H-chemisorption to 2D-Xenes.[37]

The handful of emerging reports on the role of surface termination on electronic properties of functionalized Xenes indicate that both the size and the electron-donating/electron-withdrawing properties of the ligand have a strong influence on the electronic structure. First, surface-terminating Xenes with ligands that have relatively larger van der Waals radii can produce tensile strain in the 2D framework. This tensile strain will lower the energy of the ligand-Si/Ge/Sn s-orbital antibonding levels at the conduction band maximum (CBM), effectively reducing the band gap.[12] Increasing the alkyl length by just a single methylene unit to ethyl ($–CH_2CH_3$) limits the fraction of surface atoms that are functionalized with the organic substituent to functionalization to 80-85% whereas the remaining atoms are –H terminated.[38] While the framework of functionalized Xenes might have the flexibility to accommodate the strain induced by larger ligands, to date, $GeCH_3$ is the only synthesized Xene functionalization with nearly uniform organic functionalization.[34] Second, more electronegative ligands will withdraw electron density from the Xane framework, and similarly lower the energy of the ligand-

Si/Ge/Sn s-orbital antibonding levels at the CBM.[39] Consequently, replacing the –H ligand in germanane with the more electron-donating $–CH_3$ ligand will increase the observed band gap from 1.54 to 1.67.[12,34] These Xanes can be in the form of multi-layered crystals whose length and width is determined by the size of precursor Zintl phases and can be greater than millimeters, suitable for exfoliation and further device processing.[31]

The *triple S-factor* in the epitaxial 2D-Xenes. The experimental realization of the epitaxial Xenes has been generally conditioned by three factors: Synthesis, Substrate, and Stability. This *triple S-factor* brings several challenges for a full exploitation of Xene and access to a broad range of characterization and/or applications. The synthesis of 2D-Xene is restricted to expensive molecular beam epitaxy (MBE) methodologies requiring ultra-high vacuum conditions. Moreover, substrates enabling the 2D-Xene epitaxy must be commensurate with the FS 2D-Xene structure.[14,15,16,17,19] Further efforts are in progress to design or synthesize 2D-Xenes on weakly interacting substrates, and the option of chalcogenide templates with a selected termination is promising to host a 2D-Xene lattice.[40] This is the case of the growth of hexagonal silicene sheets on semiconducting MoS_2.[41,42] The option of Xenes on non-metallic substrates would bring obvious benefits for device integration, scientific studies, and applications, and *substrate engineering* is a demanding task of technological interest.

On the other hand, the chemical stability of 2D-Xenes under ambient condition is severely restricted by the inherent thermodynamic preference of Si, Ge, and Sn for sp^3 bonding. Air-stability issues can be overcome by making use of a non-destructive encapsulation material such as Al_2O_3.[43]

The case of silicene can be taken as a paradigmatic pathway to overcome the "triple S factor" and develop a prototypical 2D-Xene nanoelectronic platform (**Figure 1e**). A silicene sheet can be sandwiched in between two thin layers, the native Ag on one side and Al_2O_3 encapsulation on the other side. The former layer comes from the delamination of the "substrate", a cleavable Ag(111)-on-mica where the silicene is epitaxially grown. The latter one is the stabilizing encapsulation sequentially deposited after silicene growth. The "silicene sandwich" is easily handled as a sheet to be placed upside down on a device-friendly platform, such as SiO_2/Si, and the top Ag patterned so as to obtain a Ag-free silicene channel in between two (or more) "native" Ag electrodes, hence completing a transistor device structure. Room temperature operation of this silicene transistor revealed an ambipolar character in agreement with the predicted graphene-like nature of the particular silicene phase in the experiment.[44] Despite the fast degradation of exposed Ag-free silicene in ambient condition that is yet to be fully addressed, this transfer methodology can be generally extended to the class of Xenes-on-substrate, and hence, offer a universal route for verifying the quantum transport properties of Xenes.[45]

Topology as a paradigm shift for quantum electronics

2D TIs support the intriguing quantum spin Hall (QSH) effect, characterized by insulating bulk states with gapless helical edge states that are protected against back-scattering by time reversal symmetry (**Figure 2a).** The QSH effect was first theoretically predicted and subsequently experimentally observed in a HgTe quantum well.[46,47] Graphene was proposed to have the same effect,[10] but its bulk gap is extremely small (~μeV). The buckled 2D-Xenes have much larger QSH gaps (up to 0.3 eV),[12] suitable for

238 room-temperature usage, and their QSH states are tunable by chemical functionalization
239 from π orbital states to σ orbital states (**Figure 2b)**.[12] This tunable topology affords an
240 electronic switch where the logic state is dictated by the topological phase transition
241 rather than by the charge depletion/inversion as in conventional semiconductors.

242 **The benefit of gaining weight.** 2D-Xenes share the same Dirac physics as
243 graphene, which is a 2D Dirac semimetal when excluding the SOC and becomes a QSH
244 insulator when including the SOC (**Figure 2b**, left).[10,9,12] Notably, the SOC-induced bulk
245 gap in silicene (1.5-2 meV)[45,9] is much larger than in graphene (~μeV). The underlying
246 mechanism is two-fold. The first-order contribution of SOC, which is turned off in a
247 planar structure like graphene, is turned on in silicene because the hybridization between
248 π and σ orbitals of nearest neighbors becomes allowed in a buckled structure.[9] Moreover,
249 the SOC strength is commensurate with increasing weight. Thus enhanced SOC is
250 obtained in germanene (23.9-30.0 meV) and stanene (~0.1eV).[9,12,48] In perspective, the
251 QSH gap increases five orders of magnitude from graphene to stanene, compliments of
252 the heavier mass and structural buckling.

253 The chemical functionalization of 2D-Xenes provides an additional degree of freedom to
254 tune topological states. The saturation of the p_z orbitals opens a large energy gap at the K
255 and K' points, which destroys the Dirac physics of the π orbitals. The low-energy physics
256 is then determined by the σ orbitals around the Γ point (**Figure 2b**, right), where inverted
257 band structures may occur in 2D-Xenes composed of heavier elements.[12,48]. Take the
258 fluorinated stanene (F-stanene) as an example. The relevant states around the Fermi level
259 are comprised of *s*, p_x, and p_y orbitals on the Sn atoms, split into bonding and anti-
260 bonding states by the Sn-Sn interaction. Unlike undecorated graphene, the anti-bonding *s*

state is located below the bonding p_{xy} state at the Γ point, showing an inverted band order. The *s*-*p* band inversion results in a nontrivial QSH phase,[12] similar to the scenario of the HgTe quantum well.[46] Therefore, the QSH states are varied from π orbitals described by the Kane-Mele model[10] to σ orbitals described by the Bernevig-Hughes-Zhang model[46].

The new QSH states derived from σ orbitals possess many advantages[12,48]. First, the QSH gaps are extraordinarily large (up to 0.3 eV), since the effective SOC of σ orbitals is significantly larger than that of π orbitals. Second, the electronic properties can be controllably tuned. Functionalization with different chemical groups can result in topologically distinct phases (**Figure 2c**). Moreover, applying external strain can effectively control the emergence or disappearance of the helical edge states.

Third, in comparison with the π orbitals that are easily affected by substrate and adsorbates,[27,49] the σ orbitals that are composed of in-plane p_{xy} states are relatively more environmentally stable. Even when forming chemical bonds with the substrate, large-gap σ-orbital-derived QSH states are predicted to be preserved in functionalized stanane[40].

Given the dependence on external factors owing to their buckled nature, 2D-Xenes may offer a high degree of functional versatility. For example, in silicene, physical influences such as electric and magnetic fields, mechanical strain, and temperature has been predicted to produce a variety of electronic states including semimetallic, semiconducting, superconducting, and trivial insulating phases, in addition to about *sixteen* 2D TI phases.[50] These TI phases arise from the combination of the four defining topological numbers in a honeycomb lattice, which are the Chern, spin-Chern, valley-Chern and spin-valley-Chern numbers with an end result of five types of topological quantum states, namely the spin-polarized quantum anomalous Hall (SQAH), quantum

284 valley Hall (QVH) and quantum spin-valley Hall (QSVH) states in addition to the already
285 mentioned QSH and QAH states (**Figure 2d**).[51]

286

287 ## A Buckled Outlook

288 The interplay of non-trivial 2D topological features and the buckled structure of 2D-
289 Xenes may also open new routes for disruptive applications like low-energy electronics,
290 piezo-magnetism, enhanced thermoelectricity and spintronics.[12] Furthermore, by
291 explicitly breaking the symmetries (for example, gauge symmetry, inversion symmetry
292 and time reversal symmetry), new emerging physics (such as topological
293 superconductivity[52], valley-polarized metal,[45] and QAH effect[45]) can be explored in 2D-
294 Xenes.

295 **From digital to topological bits.** One of the more visionary outlook about 2D-Xenes is
296 the realization of a paradigm shift from conventional to quantum electronics based on
297 field-controllable topological properties. Transport through the QSH edge states can be
298 ballistic, thus promising an exceptional advance in terms of energy saving in electronic
299 devices. In contrast to carbon nanotubes or graphene where ballistic transport can be
300 affected by defects, transport in 2D-Xenes in the QSH regime is robust against scattering.
301 Equally appealing is the opportunity to access a logic functionality based on the concept
302 of topological phase transitions. A topological phase transition occurs when the QSH
303 state characterized by ballistic edge states that can serve as information carriers ("ON"
304 state) is switched to a trivial insulator state with vanishing conductance ("OFF" state) vis-
305 à-vis an external electric field E_z (**Figure 3a**, top diagram).[50] The two ON/OFF states
306 define a logic switch mechanism, namely a *topological bit*, which can be distinguished by

307 the sequential topological gap closing and trivial gap opening as a function of the external
308 field.
309 A prototypical device structure based on the gate bias modulation can be understood as a
310 *quantum* topological insulator field-effect transistor (TI-FET)[53] as shown in the
311 corresponding sketch of **Figure 3b**. The gate bias can be employed to switch the TI-FET
312 from the ON to the OFF state, whereas the drain-source voltage facilitates one kind of
313 helical carrier through each edge. Being topologically protected and helical in character,
314 the edge states in these quantum TI-FETs serve as truly one-dimensional, spin-polarized
315 dissipationless highways for charge transport that is robust against scattering from non-
316 magnetic material defects,[12] and potentially suitable for scaled low-power nanoelectronic
317 devices.
318 The main challenge with devices based on electric field-driven topological phase
319 transitions is the relatively large critical field required ($E_c = 2\lambda_{SO}/\delta$, where $2\lambda_{SO}$ is the
320 SOC induced bandgap), which is of the order of 0.05 V/nm and 1 V/nm for silicene and
321 stanene, respectively. In light of this, a *classical* TI-FET not predicated on topological
322 phase transitions was recently proposed.[54] In this scheme, the 2D TI is configured as a
323 nanoribbon FET with the width small enough to ensure inter-edge elastic scattering
324 (namely, within an order of magnitude of the field-dependent edge-bulk tunneling length
325 scale, ~1 nm for F-stanene and ten times larger in silicene). Unlike the conventional FET
326 where the field-effect enhances the carrier density and conductivity increases, the field-
327 effect in classical TI-FET facilitates phonon-mediated scattering of edge electrons into
328 bulk states by reducing the energy barrier and hence, conductivity decreases.

Alternatively, a topological phase transition can be driven by applying external strain in functionalized 2D-Xenes because the *s-p* band inversion at the Γ point sensitively depends on the interatomic bond length.[12] In this case, the details of the topological phase transition depend on the identity of the functional group. For instance, F-stanene is a QSH insulator that undergoes a transition to a trivial insulator state as a function of the compressive strain (over a critical value of about -7%) thus nominally mimicking the same ON/OFF sequence of the electric field induced topological phase transition (**Figure 3a**, middle diagram). Conversely, H-stanene is a trivial insulator at zero applied strain and enters a QSH state when applying a tensile strain over a critical value of about 2% thus manifesting an inverted OFF-ON logic mechanism (**Figure 3a**, bottom diagram). Both mechanisms may open unprecedented routes for 2D-Xene-based piezotronic devices (see the corresponding sketches in **Figure 3b**).

New emerging applications. The existence of large-gap, tunable and robust QSH states make 2D-Xenes promising for various applications (**Figure 3c**). The large bulk gap (~0.3 eV)[12] enables QSH phenomena to occur at room temperature. The helical edge states are useful for low-energy electronics, since they can conduct electricity without generating heat[10,46,47]. They can also induce anomalous Seebeck effect due to the strong energy dependence in lifetime introduced by the edge-bulk interaction.[55] The thermoelectric performance of QSH insulators can be effectively improved by optimizing the morphology to maximize the edge-state contribution.[55] In addition, the helical edge states may also find important applications in spintronics (for example in spin transfer torque, spin Seebeck, spin-charge conversion, and spin-filter[56] based devices). However, very little experimental progress has been achieved until now, mainly because high-

quality samples are still lacking.[27] More experimental effort is thus essential to advance 2D-Xenes and related materials, and ultimately realize the above-mentioned concepts.

New emerging physics. 2D-Xenes may also offer an ideal platform to study new emerging physics. Exotic quantum effects would emerge upon explicitly breaking different symmetries in 2D-Xenes (**Figure 3c**). For instance, breaking the *inversion symmetry* by substrate or electric field introduces the Rashba effect, which enables the spin manipulation as well as access to topological superconductivity.[52] Breaking *time reversal symmetry* by magnetism[40,57] may induce the QAH effect, which supports chiral edge states that are topologically protected against scattering. A near room-temperature QAH effect has been predicted in half-functionalized stanene and germanene, where a ferromagnetic order is formed between local magnetic moments of unsaturated p_z states.[57] Breaking *gauge symmetry* by superconductivity may afford exotic topological superconducting states bearing Majorana fermions that are useful for fault-tolerant topological quantum computation.[52]

Even richer physics is expected by breaking different symmetries simultaneously. For instance, the use of an electric field together with an exchange field ΔM (from magnetic impurities or by proximity coupling with a ferromagnet) enables tuning the spin and valley degrees of freedom independently, which generates a variety of phases in 2D-Xenes.[45] Furthermore, the symmetries can be broken either globally or locally. The local symmetry breaking, though preserving the topology, can considerably affect properties of the QSH states. As an example, the helical edge states are eliminated when introducing an in-plane ferromagnetic order to the edge atoms. The existence of the helical edge

states thus can be controlled by local edge manipulation, which leads to potential applications in giant magnetoresistance and an ideal spin filter.[56]

Perspective

By virtue of their buckled character, 2D-Xenes can potentially serve as a nanotechnology platform with multiple physical features for fundamental research and applications. The diverse material properties in intrinsic and functionalized Xenes permit a wide degree of freedom in designing efficient, on-demand or reconfigurable devices for electronic, spintronic, photonic, thermal, energy, mechanical, chemical and sensor nanosystems. However, many processing and technological issues are yet to be solved, the most significant of which is the instability in ambient conditions which complicates the establishment of scalable routes for device integration schemes. Appropriate solutions including the design of device-friendly and neutral substrates, and the development of large-scale production methodologies (for example chemical vapor deposition) are demanding issues for a viable Xene nanotechnology. Nonetheless, the recently reported technological and synthetic advances are encouraging towards the exploration of the unique topological phenomena in 2D-Xenes and their exploitation in innovative device concepts.

Acknowledgements

The Authors are grateful for fruitful discussions with Dr. C. Grazianetti, E. Cinquanta, Dr. L. Tao, Prof. M. Fanciulli, Prof. V.V. Afanas'ev, Prof. A. Stesmans, Prof. William Vandenberghe, Prof. M. Fischetti, Dr. A. Dimoulas, Dr. D. Tsoutsou, and Prof. Motohiko Ezawa. The Authors thank Jo Wozniak of UT-Austin TACC center for the renderings of Fig. 3. A.M. is partially supported by the CNR under the grant "Laboratori Congiunti" (SFET project). J.G. acknowledges partial support from the Center for Emergent Materials: an NSF MRSEC under award number DMR-1420451, partial support from NSF EFRI-1433467, and the Camille and Henry Dreyfus Foundation. M.H acknowledges financial support from the KU Leuven Research Funds, project GOA/13/011. A.M. and M.H. also acknowledge partial financial support from the EU-FP7 FET-Open grant no. 270749 ("2D-Nanolattices" project). Y.X. acknowledges support from Tsinghua University Initiative Scientific Research Program and the National Thousand-Young-Talents Program. S.C.Z. is supported by the Department of Energy, Office of Basic Energy Sciences, Division of Materials Sciences and Engineering, under contract DE-AC02-76SF00515 and by FAME, one of six centers of STARnet, a Semiconductor Research Corporation program sponsored by MARCO and DARPA. D.A acknowledges support from the Army Research Office (ARO), the Presidential Early Career Award for Engineers and Scientists (PECASE), and the Gordon and Betty Moore Foundation.

Item Captions

Table 1. Properties of 2D-Xenes. Computed structural parameters of FS 2D-Xenes, using first-principles calculations based on density functional theory (left-hand side). Experimentally observed or calculated structural parameters of epitaxial Xenes-on-substrates (right-hand side). a_X, $\ell_{X\text{-}X}$, and δ are the cell lattice constant, interatomic distance, and buckling parameter in 2D-Xenes. E_g is the SOC-induced band gap. The latter branch includes a list of substrates that have been found to accommodate specific 2D-Xene lattices and their atomic reconstructions (commonly denoted as "phases") on the substrates' surface. Graphene parameters are reported for comparison. Note that graphene has nominally zero atomic buckling in the absence of rippling.

Figure 1: The 2D-Xene Odyssey. An evolutionary overview of the key-experimental evidences of 2D-Xenes. (a) Atomic configuration of a FS 2D-Xene lattice (top: side view, bottom: perspective view) where red and orange spheres represent X atoms at top and bottom positions, respectively. (b) Silicene epitaxy on Ag(111) substrates as a representative case of Xene-on-substrate systems. STM investigations of Silicene-on-Ag(111) has revealed a multiphase character. Left: The STM topographies of three majority phases, 3×3/4×4, √7×√7/√13×√13, and √7×√7/2√3×2√3, are reported along with the atomic structure models. (c) Topotactic exfoliation of germanane as a first example of the chemical exfoliation of a Xane sheet: process schematics (left) and optical microscopy image of a single hydrogen-terminated germanane sheet (right). (d) Representative case of germanene on metal substrates: STM topography of an extended

438 germanene sheet on Al(111) assisted by an *ab initio* atomic model. Adapted from Ref.[24].
439 (e) Silicene integration into a transistor device after Ref. [44]: Silicene is epitaxially grown
440 on a cleavable Ag-on-mica substrate via MBE, encapsulated with a protective Al_2O_3 and
441 then delaminated as a Al_2O_3/silicene/Ag sandwich sheet; this "silicene sandwich" is
442 transferred to a device-friendly substrate (such as SiO_2/Si) and then integrated as the
443 active channel in a field-effect transistor structure by patterning the native Ag to make
444 contact electrodes. (f) Epitaxy of stanene on Bi_2Te_3 substrates based on STM
445 identification of a buckled and unreconstructed lattice structure. Adapted from Ref. [27].

446

447 **Figure 2: Topology as a paradigm shift in nanoelectronics. a)** Top view of a 2D-
448 Xene in a QSH state bearing helical currents at the edges. **b)** Side view of the atomic
449 structure and molecular orbital, and the low-energy bands with (red solid lines) and
450 without (black dashed lines) spin-orbit coupling for pure (left) and functionalized (right)
451 Xene. The red and blue spheres denote atoms of different sublattices, and the white
452 spheres denote the chemical functional group. **c)** Energy gap as a function of the lattice
453 constant induced by the covalent functionalization of stanene. Adapted from Ref.[12].**d)**
454 The topological phase diagram as a function of perpendicular electric field E_z and the
455 exchange field ΔM, and the arrows reflect the spin polarization. Adapted from Ref.[51]

456

457 **Figure 3: The topological bit and emerging physics based on broken symmetry.**
458 **a)** Schematic band structure diagrams of nanoribbons along the 1D Brillouin zone (Γ-X',
459 X' is a *k*-point point along the nanoribbon length direction) for (top) bare stanene,
460 (middle) and fluorine-terminated (SnF), and (bottom) hydrogen-terminated (SnH) stanane

and topological phase transitions induced by an out-of-plane electric field or a compressive/tensile strain. The helical edge states that emerge within the bulk gap are denoted by red lines. **b)** Corresponding sketches of a *quantum* TI-FET driven by an electric field, by a compressive strain, and by a tensile strain. A 2D-Xene ribbon is embedded in between a top gate and a substrate (for applying V_G), and source (S) and drain (D) electrodes. **c**) Applications of the QSH states and new emerging physics induced by breaking symmetries, including the A-B sublattice symmetry, inversion symmetry *P*, time reversal symmetry *T* and gauge symmetry *U*.

484

	FS 2D-Xenes (predicted)					Epitaxial 2D-Xenes (Xene-on-substrate)					
	a_X (Å)	ℓ_{X-X} (Å)	δ (Å)	E_g	Ref.	substrate	phase	a_X (Å)	ℓ_{X-X} (Å)	δ (Å)	Ref.
Graphene	2.47	1.42	0	~1 μeV		metals		2.47	1.42	0	58
Silicene	3.87	2.28	0.44	1.5-2 meV	59	Ag(111)	3×3/4×4	11.78	2.34-2.39	0.71-0.79	14,15, 16,17
							√7×√7/√13×√13	10.60	2.31-2.36	0.77-0.79	
							√7×√7/2√3×2√3	10.20	2.28-2.37	1.10	
						Ir(111)	√3×√3/√7×√7	7.20	2.10	0.83	18
						ZrB_2	√3×√3/2×2	6.72-6.78	2.24-2.26	0.90-1.35	19
						MoS_2	1×1/1×1	3.17	2.61	1.90	41
Germanene	4.06	2.44	0.69	23.9-30.0 meV	59	Au(111)	√3×√3/√7×√7	7.65	2.55	0.47	22
						Pt(111)	3×3/√19×√19	12.0	~2.31	0.60	23
						Al(111)	2×2/3×3	8.50	2.58	1.23	24
						MoS_2	1×1/1×1	3.82	2.20	0.86	42
						hex-AlN	3×3/4×4	12.31	2.37	0.70	26
Stanene	4. 68	2.83	0.85	0.1 eV	12	Bi_2Te_3	1×1/1×1	4.38	2.80	1.20	27

485

486

487

488 **Table 1**

489

490

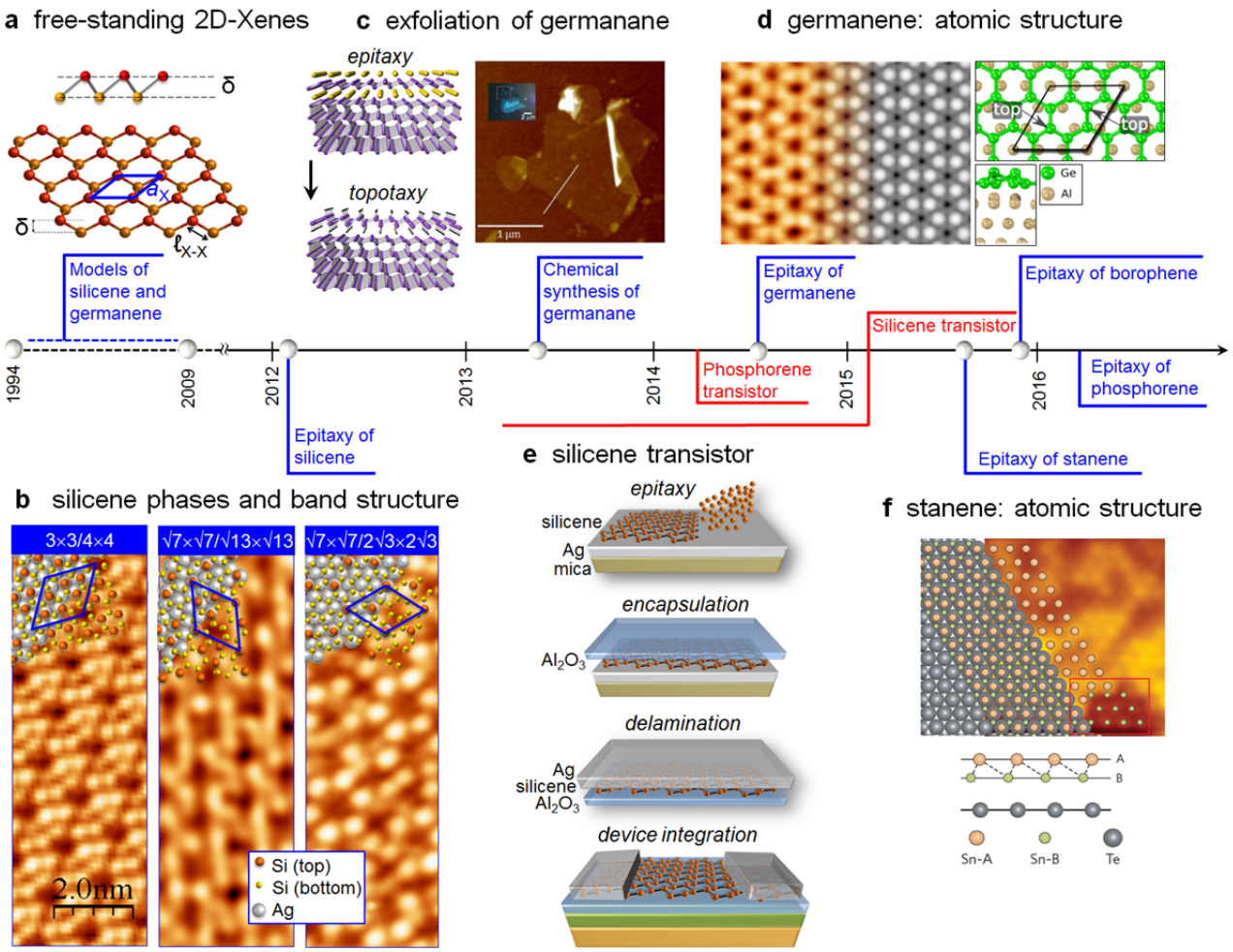
a free-standing 2D-Xenes
δ
δ
a_{X-X}
c exfoliation of germanane
epitaxy
topotaxy
1 μm
d germanene: atomic structure
top
top
Ge
Al
Models of silicene and germanene
Chemical synthesis of germanane
Epitaxy of germanene
Silicene transistor
Epitaxy of borophene
1994
2009
2012
2013
2014
Phosphorene transistor
2015
2016
Epitaxy of phosphorene
Epitaxy of silicene
Epitaxy of stanene
b silicene phases and band structure
3×3/4×4
√7×√7/√13×√13
√7×√7/2√3×2√3
2.0nm
Si (top)
Si (bottom)
Ag
e silicene transistor
epitaxy
silicene
Ag
mica
encapsulation
Al_2O_3
delamination
Ag
silicene
Al_2O_3
device integration
f stanene: atomic structure
A
B
Sn-A
Sn-B
Te

Figure 1

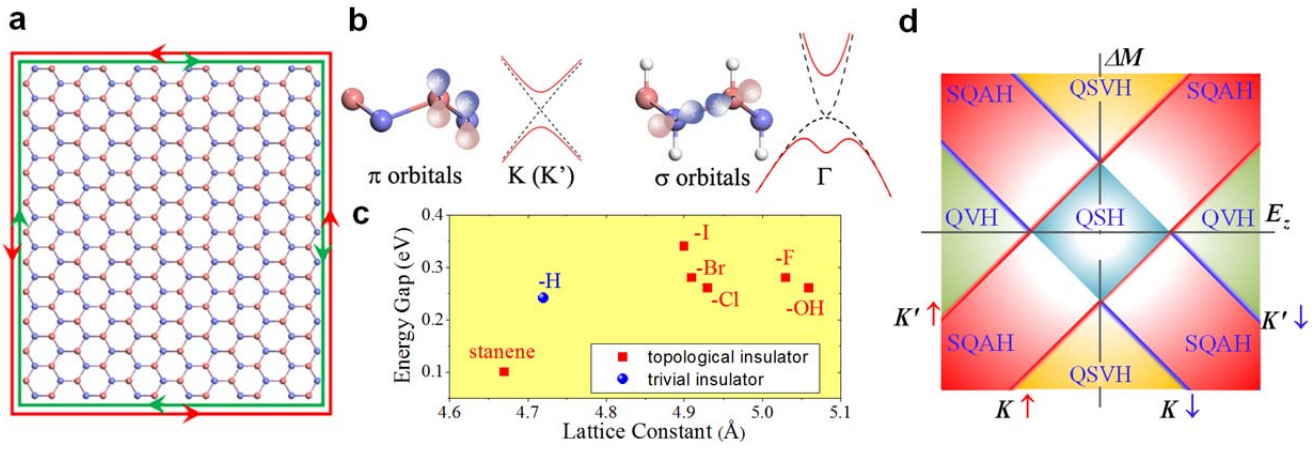
a
b
π orbitals
K (K')
σ orbitals
Γ
c
Energy Gap (eV)
Lattice Constant (Å)
-I
-Br
-Cl
-F
-OH
-H
stanene
topological insulator
trivial insulator
d
ΔM
SQAH
QSVH
QVH
QSH
E_z
K′↑
K′↓
K↑
K↓

Figure 2

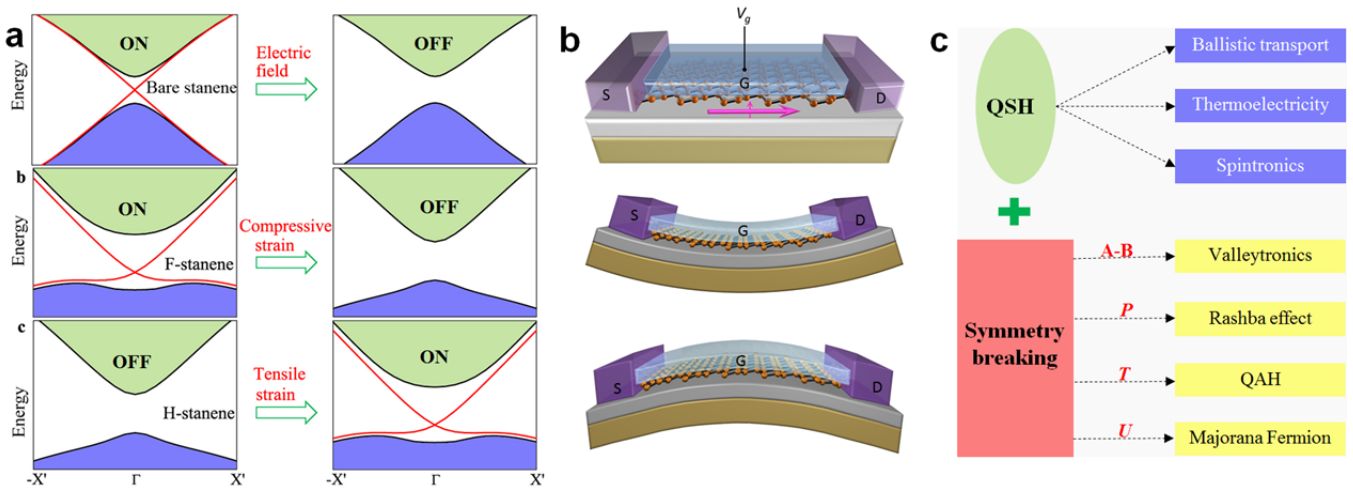
a
ON
Bare stanene
Energy
Electric field
OFF
b
ON
F-stanene
Compressive strain
OFF
c
OFF
H-stanene
Tensile strain
ON
-X'
Γ
X'
b
V_g
S
G
D
c
QSH
Ballistic transport
Thermoelectricity
Spintronics
Symmetry breaking
A-B
Valleytronics
P
Rashba effect
T
QAH
U
Majorana Fermion

Figure 3

List of References

[1] G Fiori, F Bonaccorso, G Iannaccone, T Palacios, D Neumaier, A Seabaugh, SK Banerjee, and L Colombo, Nature Nanotechnology **9** (10), 768 (2014).

[2] AC Ferrari, F Bonaccorso, V Fal'ko, KS Novoselov, S Roche, P Boggild, S Borini, FHL Koppens, V Palermo, N Pugno, JA Garrido, R Sordan, A Bianco, L Ballerini, M Prato, E Lidorikis, J Kivioja, C Marinelli, T Ryhanen, A Morpurgo, JN Coleman, V Nicolosi, L Colombo, A Fert, M Garcia-Hernandez, A Bachtold, GF Schneider, F Guinea, C Dekker, M Barbone, ZP Sun, C Galiotis, AN Grigorenko, G Konstantatos, A Kis, M Katsnelson, L Vandersypen, A Loiseau, V Morandi, D Neumaier, E Treossi, V Pellegrini, M Polini, A Tredicucci, GM Williams, BH Hong, JH Ahn, JM Kim, H Zirath, BJ van Wees, H van der Zant, L Occhipinti, A Di Matteo, IA Kinloch, T Seyller, E Quesnel, XL Feng, K Teo, N Rupesinghe, P Hakonen, SRT Neil, Q Tannock, T Lofwandera, and J Kinaret, Nanoscale **7** (11), 4598 (2015).

[3] Akinwande D, Tao L, Yu Q, Lou X, Peng P, and Kuzum D, IEEE Nanotechnology Magazine **9**, 6 (2015).

[4] S Balendhran, S Walia, H Nili, S Sriram, and M Bhaskaran, Small **11**, 640 (2015).

[5] K Takaeda and K Shiraishi, Physical Review B **50**, 14916 (1994).

[6] S Cahangirov, M Topsakal, E Akturk, H Sahin, and S Ciraci, Physical Review Letters **102**, 236804 (2009).

[7] GG Guzman-Verri and LCLY Voon, Physical Review B **76**, 075131 (2007).

[8] Carlo Grazianetti, Eugenio Cinquanta, and Alessandro Molle, 2d Materials **3** (1) (2016).

[9] CC Liu, WX Feng, and YG Yao, Physical Review Letters **107** (7), 076802 (2011).

[10] CL Kane and EJ Mele, Physical Review Letters **95**, 146802 (2005).

[11] M Houssa, A Dimoulas, and A Molle, Journal of Physics-Condensed Matter **27**, 253002 (2015).

[12] Y Xu, BH Yan, HJ Zhang, J Wang, G Xu, PZ Tang, WH Duan, and SC Zhang, Physical Review Letters **111**, 136804 (2013).

[13] B van den Broek, M Houssa, E Scalise, G Pourtois, VV Afanas'ev, and A Stesmans, 2D Materials **1**, 021004 (2014).

[14] P Vogt, P De Padova, C Quaresima, J Avila, E Frantzeskakis, MC Asensio, A Resta, B Ealet, and G Le Lay, Physical Review Letters **108**, 155501 (2012).

[15] CL Lin, R Arafune, K Kawahara, N Tsukahara, E Minamitani, Y Kim, N Takagi, and M Kawai, Applied Physics Express **5**, 045802 (2012).

[16] BJ Feng, ZJ Ding, S Meng, YG Yao, XY He, P Cheng, L Chen, and KH Wu, Nano Letters **12**, 3507 (2012).

[17] Daniele Chiappe, Carlo Grazianetti, Grazia Tallarida, Marco Fanciulli, and Alessandro Molle, Advanced Materials **24**, 5088 (2012).

[18] L Meng, YL Wang, LZ Zhang, SX Du, RT Wu, LF Li, Y Zhang, G Li, HT Zhou, WA Hofer, and HJ Gao, Nano Letters **13**, 685 (2013).

[19] A Fleurence, R Friedlein, T Ozaki, H Kawai, Y Wang, and Y Yamada-Takamura, Physical Review Letters **108**, 245501 (2012).

[20] E Scalise, E Cinquanta, M Houssa, B van den Broek, D Chiappe, C Grazianetti, G Pourtois, B Ealet, A Molle, M Fanciulli, VV Afanas'ev, and A Stesmans, Applied Surface Science **291**, 113 (2014).
[21] Tsoutsou D, Xenogiannopoulou E, Golias E, Tsipas P, and Dimoulas A, Applied Physics Letters **103**, 231604 (2013).
[22] ME Davila, L Xian, S Cahangirov, A Rubio, and G Le Lay, New Journal of Physics **16**, 095002 (2014).
[23] LF Li, SZ Lu, JB Pan, ZH Qin, YQ Wang, YL Wang, GY Cao, SX Du, and HJ Gao, Advanced Materials **26**, 4820 (2014).
[24] M Derivaz, D Dentel, R Stephan, MC Hanf, A Mehdaoui, P Sonnet, and C Pirri, Nano Letters **15**, 2510 (2015).
[25] P Bampoulis, L Zhang, A Safaei, R van Gastel, B Poelsema, and HJW Zandvliet, Journal of Physics-Condensed Matter **26**, 442001 (2014).
[26] F D'Acapito, S Torrengo, E Xenogiannopoulou, P Tsipas, J Marquez Velasco, D Tsoutsou, and A Dimoulas, Journal of Physics - Condensed Matter (2016).
[27] FF Zhu, WJ Chen, Y Xu, CL Gao, DD Guan, CH Liu, D Qian, SC Zhang, and JF Jia, Nature Materials **14**, 1020 (2015).
[28] AJ Mannix, XF Zhou, B Kiraly, JD Wood, D Alducin, BD Myers, XL Liu, BL Fisher, U Santiago, JR Guest, MJ Yacaman, A Ponce, AR Oganov, MC Hersam, and NP Guisinger, Science **350** (6267), 1513 (2015).
[29] Baojie Feng, Jin Zhang, Qing Zhong, Wenbin Li, Shuai Li, Hui Li, Peng Cheng, Sheng Meng, Lan Chen, and Kehui Wu, Nat Chem **advance online publication** (2016).
[30] Jia Lin Zhang, Songtao Zhao, Cheng Han, Zhunzhun Wang, Shu Zhong, Shuo Sun, Rui Guo, Xiong Zhou, Cheng Ding Gu, Kai Di Yuan, Zhenyu Li, and Wei Chen, Nano Letters (2016).
[31] Elisabeth Bianco, Sheneve Butler, Shishi Jiang, Oscar D. Restrepo, Wolfgang Windl, and Joshua E. Goldberger, Acs Nano **7**, 4414 (2013).
[32] Shishi Jiang, Maxx Q. Arguilla, Nicholas D. Cultrara, and Joshua E. Goldberger, Accounts of Chemical Research **48** (1), 144 (2015).
[33] F. Wohler, Justus Liebigs Annalen der Chemie **127** (3), 257 (1863).
[34] Shishi Jiang, Sheneve Butler, Elisabeth Bianco, Oscar D. Restrepo, Wolfgang Windl, and Joshua E. Goldberger, Nature Communications **5**, 3389 (2014).
[35] Hideyuki Nakano, Mitsuru Nakano, Koji Nakanishi, Daiki Tanaka, Yusuke Sugiyama, Takashi Ikuno, Hirotaka Okamoto, and Toshiaki Ohta, Journal of the American Chemical Society **134** (12), 5452 (2012).
[36] XH Liang, QH Zhang, MD Lay, and JL Stickney, Journal of the American Chemical Society **133** (21), 8199 (2011).
[37] Qiu J, Fu X, Xu Y, Zhou Q, Meng S, Li H, Chen L, and Wu K, (ACS Nano, 2015), Vol. 9, pp. 11192.
[38] Hongbin Yu, Lauren J. Webb, Santiago D. Solares, Peigen Cao, William A. Goddard, III, James R. Heath, and Nathan S. Lewis, Journal of Physical Chemistry B **110**, 23898 (2006).
[39] CG van de Walle and JE Northrup, Physical Review Letters **70**, 1116 (1993).
[40] Y Xu, PZ Tang, and SC Zhang, Physical Review B **92**, 081112 (2015).

[41] D Chiappe, E Scalise, E Cinquanta, C Grazianetti, B van den Broek, M Fanciulli, M Houssa, and A Molle, Advanced Materials **26** (13), 2096 (2014).
[42] L. Zhang, P. Bampoulis, A. N Rudenko, Q. Yao, A. van Houselt, B. Poelsema, M. I Katsnelson, and H. J W Zandvliet, Physical Review Letters **116** (25), 256804 (2016).
[43] A Molle, C Grazianetti, D Chiappe, E Cinquanta, E Cianci, G Tallarida, and M Fanciulli, Advanced Functional Materials **23** (35), 4340 (2013).
[44] L Tao, E Cinquanta, D Chiappe, C Grazianetti, M Fanciulli, M Dubey, A Molle, and D Akinwande, Nature Nanotechnology **10** (3), 227 (2015).
[45] M Ezawa, Physical Review Letters **109**, 055502 (2012).
[46] BA Bernevig, TL Hughes, and SC Zhang, Science **314**, 1757 (2006).
[47] M Konig, S Wiedmann, C Brune, A Roth, H Buhmann, LW Molenkamp, XL Qi, and SC Zhang, Science **318**, 766 (2007).
[48] C Si, JW Liu, Y Xu, J Wu, BL Gu, and WH Duan, Physical Review B **89**, 115429 (2014).
[49] PZ Tang, PC Chen, WD Cao, HQ Huang, S Cahangirov, LD Xian, Y Xu, SC Zhang, WH Duan, and A Rubio, Physical Review B **90** (12) (2014).
[50] Motohiko Ezawa, Journal of the Physical Society of Japan **84** (12), 121003 (2015).
[51] M Ezawa, Physical Review B **87**, 155415 (2013).
[52] J Wang, Y Xu, and SC Zhang, Physical Review B **90**, 054503 (2014).
[53] M Ezawa, Applied Physics Letters **102**, 172103 (2013).
[54] WG Vandenberghe and MV Fischetti, Journal of Applied Physics **116**, 173707 (2014).
[55] Y Xu, ZX Gan, and SC Zhang, Physical Review Letters **112**, 226801 (2014).
[56] S Rachel and M Ezawa, Physical Review B **89**, 195303 (2014).
[57] SC Wu, GC Shan, and BH Yan, Physical Review Letters **113**, 256401 (2014).
[58] J Wintterlin and ML Bocquet, Surface Science **603** (10-12), 1841 (2009).
[59] E Scalise, M Houssa, G Pourtois, B van den Broek, V Afanas'ev, and A Stesmans, Nano Research **6** (1), 19 (2013).

	Free-standing Xenes (predicted)					Epitaxial Xenes (Xene-on-substrate)					
	a_X (Å)	$\ell_{X\text{-}X}$ (Å)	δ (Å)	E_g	Ref.	substrate	phase	a_X (Å)	$\ell_{X\text{-}X}$ (Å)	δ (Å)	Ref.
Graphene	2.47	1.42	0	~1 μeV		metals		2.47	1.42	0	58
Silicene	3.87	2.28	0.44	1.5-2 meV	59	Ag(111)	3×3/4×4	11.78	2.34-2.39	0.71-0.79	14,15, 16,17
							√7×√7/√13×√13	10.60	2.31-2.36	0.77-0.79	
							√7×√7/2√3×2√3	10.20	2.28-2.37	1.10	
						Ir(111)	√3×√3/√7×√7	7.20	2.10	0.83	18
						ZrB_2	√3×√3/2×2	6.72-6.78	2.24-2.26	0.90-1.35	19
						MoS_2	1×1/1×1	3.17	2.61	1.90	41
Germanene	4.06	2.44	0.69	23.9-30.0 meV	59	Au(111)	√3×√3/√7×√7	7.65	2.55	0.47	22
						Pt(111)	3×3/√19×√19	12.0	~2.31	0.60	23
						Al(111)	2×2/3×3	8.50	2.58	1.23	24
						MoS_2	1×1/1×1	3.82	2.20	0.86	42
						hex-AlN	3×3/4×4	12.31	2.37	0.70	26
Stanene	4. 68	2.83	0.85	0.1 eV	12	Bi_2Te_3	1×1/1×1	4.38	2.80	1.20	27

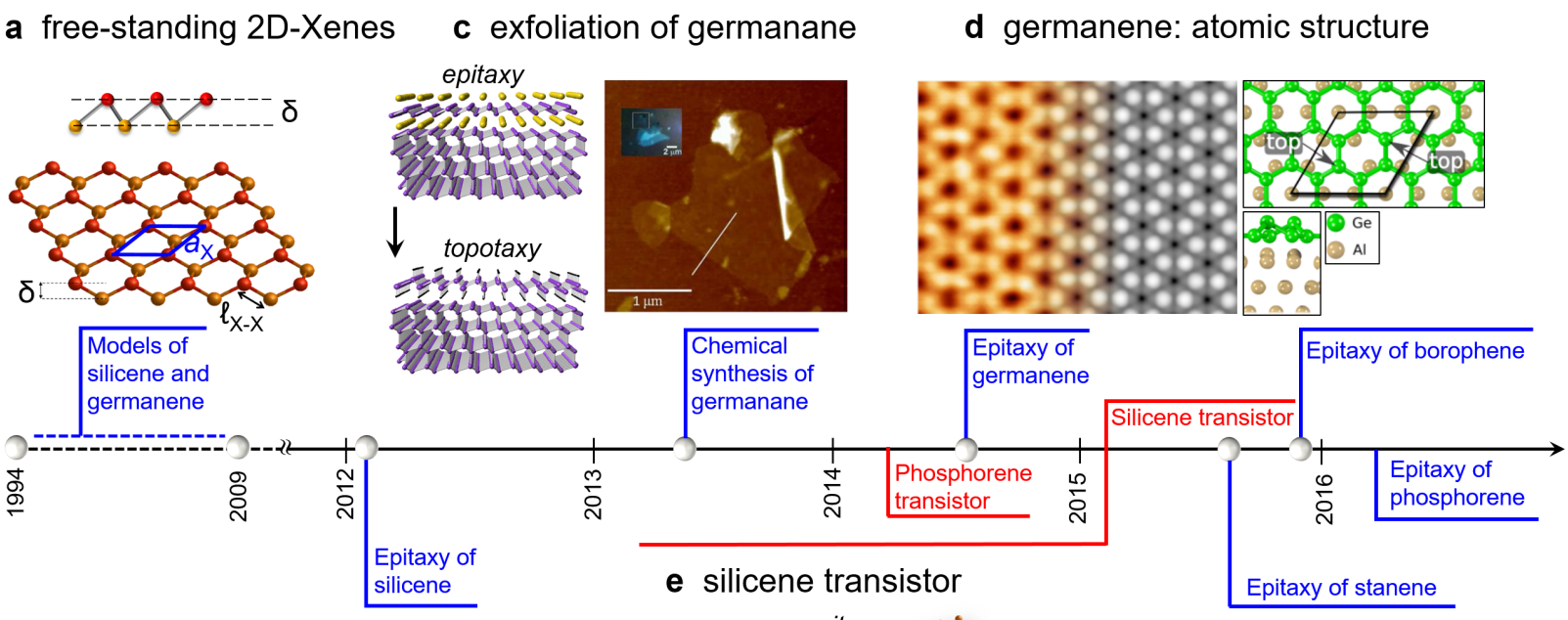
a free-standing 2D-Xenes
δ
a_X
δ
ℓ_{X-X}
c exfoliation of germanane
epitaxy
topotaxy
1 µm
d germanene: atomic structure
top
top
Ge
Al
Models of silicene and germanene
Chemical synthesis of germanane
Epitaxy of germanene
Silicene transistor
Epitaxy of borophene
1994
2009
2012
2013
2014
Phosphorene transistor
2015
2016
Epitaxy of phosphorene
Epitaxy of silicene
Epitaxy of stanene

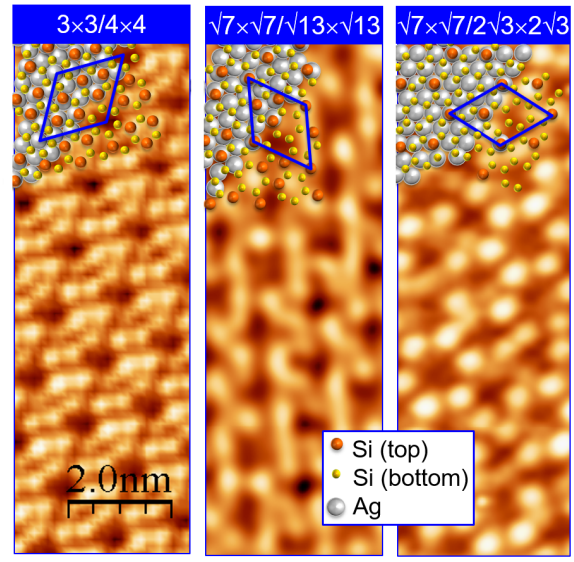
b silicene phases and band structure
3×3/4×4
√7×√7/√13×√13
√7×√7/2√3×2√3
2.0nm
Si (top)
Si (bottom)
Ag

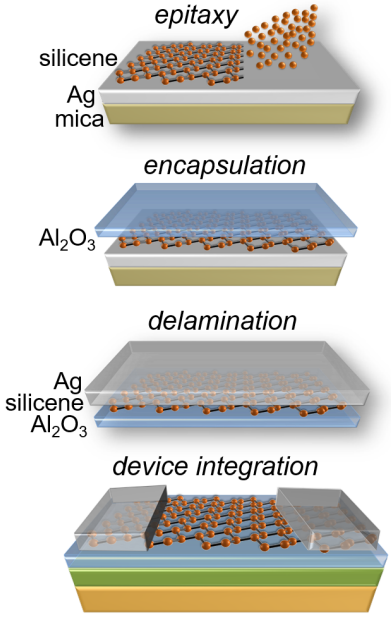
e silicene transistor
epitaxy
silicene
Ag
mica
encapsulation
Al_2O_3
delamination
Ag
silicene
Al_2O_3
device integration

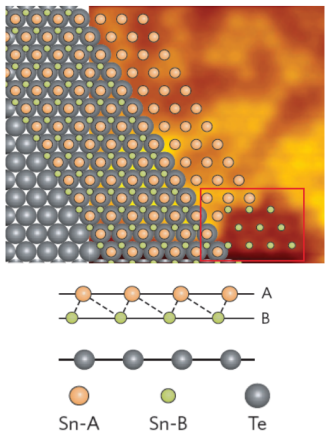
f stanene: atomic structure
A
B
Sn-A
Sn-B
Te

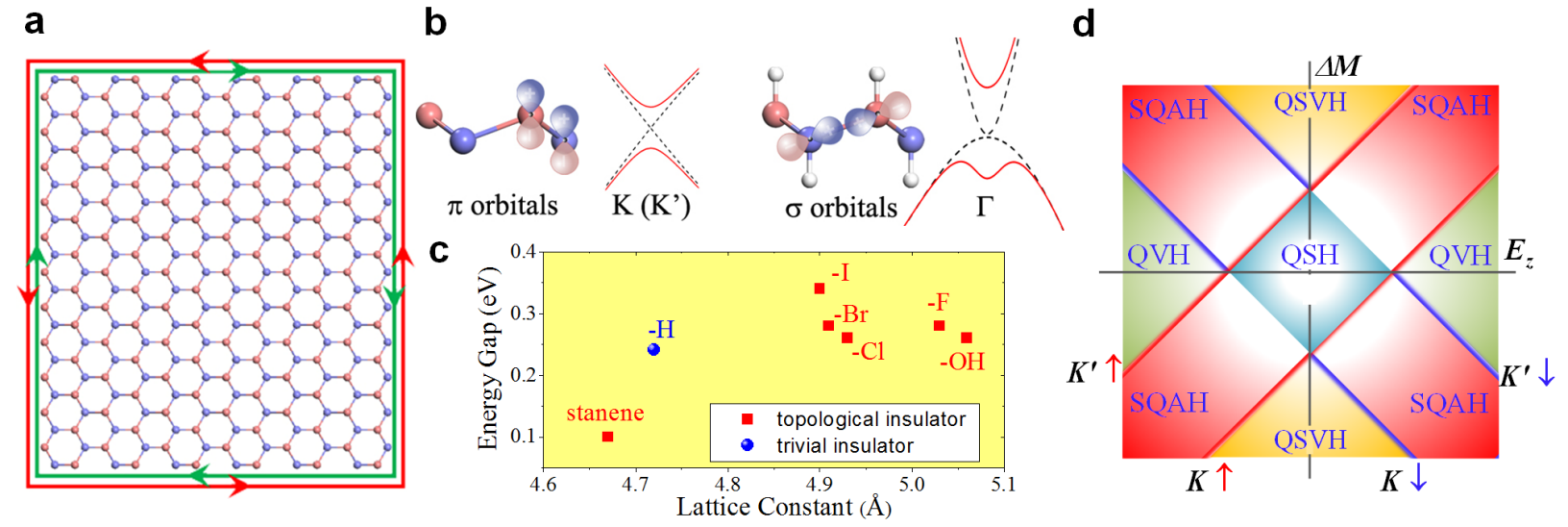
a
b
π orbitals
K (K')
σ orbitals
Γ
c
Energy Gap (eV)
0.4
0.3
0.2
0.1
4.6
4.7
4.8
4.9
5.0
5.1
Lattice Constant (Å)
-I
-Br
-Cl
-F
-OH
-H
stanene
topological insulator
trivial insulator
d
ΔM
SQAH
QSVH
SQAH
QVH
QSH
QVH
E_z
K' ↑
K' ↓
SQAH
SQAH
QSVH
K ↑
K ↓

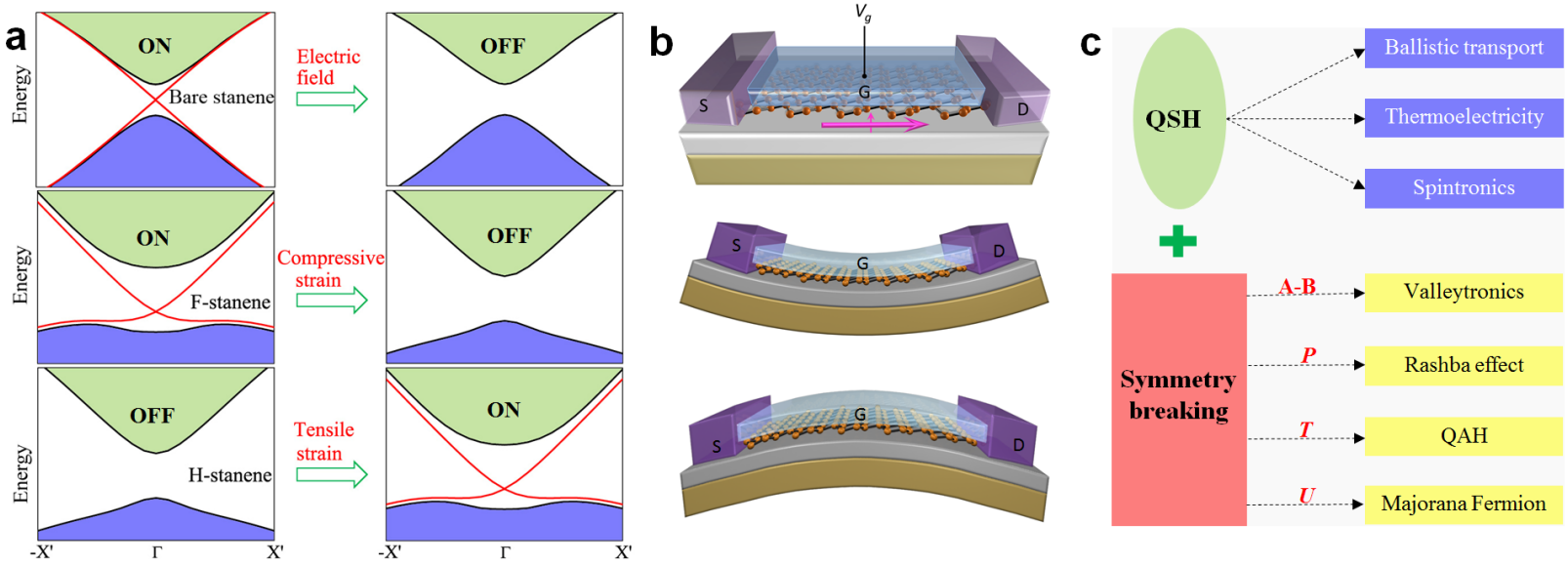
a
ON
Bare stanene
Energy
Electric field
OFF
ON
F-stanene
Energy
Compressive strain
OFF
OFF
H-stanene
Energy
Tensile strain
ON
-X'
Γ
X'
-X'
Γ
X'
b
V_g
S
G
D
S
G
D
S
G
D
c
QSH
Ballistic transport
Thermoelectricity
Spintronics
Symmetry breaking
A-B
Valleytronics
P
Rashba effect
T
QAH
U
Majorana Fermion